2025 International Conference on Electrical, Computer and Communication Engineering (ECCE), 13-15 February 2025, CUET, Chattogram-4349, Bangladesh

Mitigating Noise from Biomedical Images Using Wavelet Transform Techniques

Asadullah Bin Rahman[1], Masud Ibn Afjal[2], Md. Abdulla Al Mamun[3]
[1,2,3]Department of Computer Science and Engineering, Hajee Mohammad Danesh Science and Technology University
Dinajpur-5200, Bangladesh
[1]galib.hstu.cse17@gmail.com, [2]masud@hstu.ac.bd, [3]mamun@hstu.ac.bd

***Abstract*—Medical imaging plays a pivotal role in modern healthcare, enabling accurate diagnosis and effective treatment planning across various medical conditions. Advanced modalities, such as magnetic resonance imaging (MRI), computed tomography (CT), and ultrasound, offer critical insights into the structure and function of the human body. However, these images are often degraded by noise introduced during acquisition or processing, potentially obscuring vital diagnostic details and impacting clinical decision-making. Furthermore, enhancement techniques like histogram equalization, while improving visual appeal, may inadvertently amplify existing noise, such as salt-and-pepper distortions. This study investigates wavelet transform-based denoising methods to mitigate noise in medical images effectively. Our primary goal is to identify the optimal combination of threshold values, decomposition levels, and wavelet types to achieve superior denoising performance, ensuring enhanced diagnostic accuracy. Our study finds that the db3 wavelet with universal thresholding achieved the best denoising effect across various noise levels. For noise standard deviations of σ = 10, 15, and 25, the best PSNR values obtained are 29.203 dB, 27.791 dB, and 25.194 dB, respectively. These results establish a foundation for developing hybrid wavelet-deep learning approaches for medical image denoising.**

***Index Terms*—Image Denoising, Magnetic Resonance Imaging (MRI), Discrete Wavelet Transformation (DWT).**

I. Introduction

Noise in medical images can arise from various sources, including the imaging acquisition process itself, patient motion, and external interference. For instance, magnetic resonance imaging (MRI) images can be affected by thermal noise from the patient's body and electronic components, while computed tomography (CT) scans may suffer from quantum noise due to the limited number of X-ray photons detected. Ultrasound images are particularly susceptible to speckle noise, an inherent artifact of the coherent nature of ultrasound waves. These noise sources manifest as random fluctuations, blurring, or other distortions in the resulting images, complicating the interpretation and analysis tasks performed by radiologists and medical professionals.

To address these challenges, various image denoising techniques have been explored. Traditional approaches, such as linear filtering, wavelet-based methods, and non-local means denoising, have shown some success in reducing noise levels while preserving image features. However, these methods often struggle with complex noise patterns and may introduce undesirable artifacts or over-smoothing. For instance, Kollem et al. [1] proposed a diffusivity function-based PDE approach incorporating Quaternion Wavelet Transform and a generalized cross-validation function for threshold selection, effectively reducing noise while preserving edges. Wavelet-based methods have further evolved through innovations such as Rational Wavelet Transform (RWT), which incorporates wavelet properties into neural networks [2]. These Wavelet Neural Networks (WNNs) integrate wavelets as preprocessing steps or activation functions, enabling hybrid approaches for image denoising. Another hybrid method combining Wavelet Transform (WT) and Singular Value Decomposition (SVD) has been shown to improve the signal-to-noise ratio (SNR) and peak signal-to-noise ratio (PSNR), offering enhanced denoising performance [3]. Similarly, Zhang et al. [4] introduced a fractional-order total variation model leveraging differential operators and sparrow search algorithms to balance noise removal and texture preservation. Recent advances in deep learning have revolutionized denoising methods, offering sophisticated solutions to complex noise patterns. Autoencoders, for instance, have gained attention for their ability to learn compact representations of noisy data. Walid et al. [5] presented CADTra, a deep-learning-based autoencoder approach utilizing a Gaussian-distribution based loss function to improve noise removal and pneumonia classification. Comprehensive surveys like that of Izadi et al. [6] highlight the progression of deep denoisers, covering benchmark datasets, evaluation metrics, and both supervised and unsupervised methods. Hybrid deep learning approaches, such as MWDCNN [7], combine CNNs, Wavelet Transforms, and residual blocks to achieve superior denoising performance in natural images, with potential applications in medical imaging. Despite these advances, challenges remain. Large training data requirements, computational inefficiency, and the opaque nature of learned representations continue to limit the applicability of deep learning in denoising tasks [8].

The literature underscores the effectiveness of wavelet transforms and deep learning techniques, especially convolutional neural networks (CNNs), autoencoders, and generative adversarial networks (GANs), in the denoising of medical images. These methods effectively minimize noise while preserving essential details, thereby enhancing diagnostic accuracy and improving clinical outcomes. This research builds on these foundational concepts by exploring wavelet transform techniques specifically for denoising MRI brain images to enhance image quality and broaden diagnostic capabilities. The key

979-8-3503-5750-9/25/$31.00 ©2025 IEEE

contributions of this research include:

- Identifying the optimal configurations for MRI image denoising, with the sym4, db3, and bior6.8 wavelets demonstrating the best performance across various noise levels.
- Conducting a thorough evaluation using Peak Signal-to-Noise Ratio (PSNR), Mean Squared Error (MSE), and Structural Similarity Index (SSIM) to compare different denoising methods and their effectiveness at various noise levels.
- Laying the groundwork for combining wavelet-based denoising with deep learning techniques to create more robust solutions.

In the following sections, we discuss our approach in detail. Section II describes the used methodology. Section III presents an in-depth analysis of the dataset, parameters, and results. Finally, Section IV highlights conclusions and future research directions.

II. Methodology

Wavelet decomposition techniques have proven to be effective tools for denoising MRI images due to their multi-resolution capabilities. These techniques allow for the separation of the signal (image) from noise by decomposing the image into various frequency components, applying thresholding to reduce noise, and then reconstructing the denoised image. In this study, the wavelet decomposition method is implemented for MRI image denoising. The detailed system workflow is depicted in Figure 1.

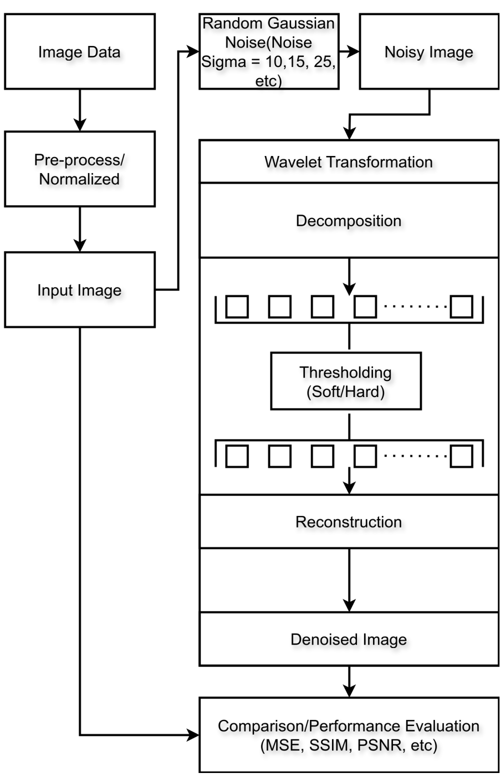

Fig. 1. A detailed system flowchart

A. *Why Wavelet Transform for Image Denoising?*

Wavelet transformation offers several key advantages that make it particularly well-suited for medical image denoising:

1) Multi-resolution Analysis: Unlike traditional filtering methods, wavelets provide simultaneous analysis at different resolution levels, allowing the preservation of important image features while effectively removing noise.
2) Localization Properties: Wavelets excel in both frequency and spatial localization, enabling more precise identification and removal of noise components while maintaining image integrity. This dual localization is especially valuable in MRI images where noise patterns can vary across different image regions.
3) Sparse Representation: Medical images have sparse wavelet domain representations, making noise-signal separation more effective than Fourier-based methods.
4) Deterministic Approach: Unlike deep learning methods requiring extensive training data and computation, wavelet-based denoising:
    - Computationally efficient with no training overhead
    - Independent of dataset availability or quality
    - Immediately applicable to new medical imaging scenarios
    - More interpretable due to its mathematical foundation
    - Consistent in performance across different implementations
5) Edge Preservation: Wavelets are particularly effective at preserving edge information while removing noise, which is crucial in medical imaging where boundary information often carries diagnostic significance.

B. *Data Collection and Preprocessing*

The MRI image dataset used in this study was sourced from figshare [9]. This dataset consists of 3,064 brain tumor MRI images, providing a diverse collection of medical images for experimentation. For the purposes of this study, a single sample was selected and prepared as follows:

1) Image Retrieval: The selected images were retrieved and loaded into the experimental setup.
2) Normalization: Pixel intensities were normalized to fall within the range of 0–255 to ensure consistency during processing.
3) Noise Addition: Since MRI images are often affected by Gaussian noise, Gaussian noise was artificially introduced with mean (μ) = 0 and standard deviations (σ) of 10, 15, and 25 to simulate real-world noise scenarios.

C. *Wavelet-based Denoising*

Wavelet decomposition techniques leverage the multi-resolution nature of wavelets to effectively denoise MRI images. By decomposing an image into different frequency components, separating the signal from noise becomes more manageable. The key steps in this process are:

1) Wavelet Transform: The MRI image is decomposed into various scales using a wavelet transform. This results in approximation coefficients (low-frequency information) and detail coefficients (high-frequency information).
2) Optimal Threshold Determination: A method is devised to determine the optimal threshold for denoising, utilizing techniques such as the Universal and Bayes methods.
3) Thresholding: The detail coefficients, which often carry noise, are processed using thresholding methods. Two commonly used approaches are hard thresholding and soft thresholding.
4) Reconstruction: The inverse wavelet transform is applied to the modified coefficients to reconstruct the denoised image.

D. Wavelet Types

Wavelets come in various types, such as orthogonal, biorthogonal, and symmetric wavelets. For this study, three wavelets: db3, bior6.8, and sym4 were considered. While orthogonal and biorthogonal wavelets are commonly used for audio signal denoising, their properties also make them suitable for image signal processing.

- Daubechies Wavelet (db3): The db3 wavelet belongs to the Daubechies family, characterized by compact support and orthogonality. With three vanishing moments, it is well-suited for capturing polynomial behavior in the data. It effectively preserves smooth regions and edges in images, balancing detail preservation and noise reduction.
- Biorthogonal Wavelet (bior6.8): The bior6.8 wavelet offers separate scaling and wavelet functions, with 6 vanishing moments for the scaling function and 8 for the wavelet function. This biorthogonal wavelet is particularly useful in image processing due to its symmetry and superior reconstruction properties, maintaining sharp edges while reducing noise.
- Symlet Wavelet (sym4): The sym4 wavelet, a modification of the Daubechies wavelet, is more symmetric and features four vanishing moments. This symmetry makes it advantageous in image processing tasks, providing a balance between noise reduction and edge retention.

E. Optimal Threshold Value Calculation

Calculating the optimal threshold is critical for effectively distinguishing between signal and noise in wavelet-based denoising. Two popular methods for determining this threshold are as follows:

1) Bayes Method: This approach minimizes the mean squared error (MSE) between the estimated and true images by leveraging the statistical properties of the noise [10]. The optimal threshold value for this method is given by:

$$\tau_{\text{bayes}} = \begin{cases} \frac{\sigma_{\text{noise}}^2}{\sigma_{\text{signal}}} & \text{if } \sigma_{\text{signal}} > 0 \\ \max(|c_j|) & \text{otherwise} \end{cases} \tag{1}$$

Where:

- τ_{bayes} is the Bayes threshold value,
- c represents the wavelet coefficients,
- $\sigma_{\text{signal}} = \sqrt{\max(\text{Var}(c) - \sigma_{\text{noise}}^2, 0)}$ estimates the signal standard deviation from the wavelet coefficients c,
- σ_{noise} is the noise standard deviation.

2) Universal Method: The Universal method provides a global threshold, simplifying the denoising process [11]. The threshold is defined as:

$$\tau_{\text{universal}} = \sigma_{\text{noise}} \sqrt{2\log(N)} \tag{2}$$

Where:

- $\tau_{\text{universal}}$ is the Universal threshold value,
- σ_{noise} is the noise standard deviation,
- N is the number of wavelet coefficients.

F. Thresholding Techniques

Thresholding is a critical step in wavelet-based denoising, where the goal is to modify wavelet coefficients to suppress noise while retaining significant signal components. This process involves either shrinking or removing coefficients based on a predefined threshold value.

1) Hard Thresholding: In hard thresholding, coefficients below a specified threshold (τ) are set to zero, while those above the threshold remain unchanged [12]. This method is defined as:

$$\hat{c}_j = \begin{cases} c_j & \text{if } |c_j| > \tau \\ 0 & \text{otherwise} \end{cases} \tag{3}$$

While hard thresholding can effectively eliminate noise, it may introduce artifacts and cause loss of detail in the reconstructed signal.

2) Soft Thresholding: In soft thresholding, coefficients are both shrunk and thresholded [12]. Coefficients smaller than the threshold are set to zero, while those exceeding the threshold are reduced in magnitude by τ. This method is expressed as:

$$\hat{c}_j = \begin{cases} 0 & \text{for } |c_j| \leq \tau \\ c_j - \tau & \text{for } c_j > \tau \end{cases} \tag{4}$$

Soft thresholding introduces smoother transitions compared to hard thresholding, which helps preserve signal continuity. However, it may result in a slight blurring effect in images.

From the above,

- c_j is the wavelet coefficient,
- τ is the optimal threshold value calculated from Bayes or Universal method,
- $\hat{c}_j$ is the modified wavelet coefficient after thresholding.

G. Performance Metrics in Image Denoising

Performance metrics are crucial for evaluating the quality of processed images. In the context of image denoising, three commonly used metrics are Mean Squared Error (MSE), Peak Signal-to-Noise Ratio (PSNR), and Structural Similarity Index

(SSIM). Each metric provides unique insights into the quality of denoised images in comparison to the original images. Together, these metrics facilitate a comprehensive evaluation of denoising algorithms.

While MSE offers a straightforward measure of error, PSNR gives a logarithmic perspective on the signal quality, and SSIM incorporates human visual perception into its evaluation.

Mean Squared Error (MSE) quantifies the average squared difference between the original and the denoised image [13]. It is calculated using the formula:

$$\text{MSE} = \frac{1}{MN} \sum_{i=1}^{M} \sum_{j=1}^{N} [I(i,j) - K(i,j)]^2 \tag{5}$$

where:

- $I(i,j)$ is the pixel value of the original image,
- $K(i,j)$ is the pixel value of the denoised image,
- M and N are the dimensions (height and width) of the images.

A lower MSE value indicates better denoising performance, as it represents a smaller error between the original and the denoised image.

Peak Signal-to-Noise Ratio (PSNR) measures the maximum signal power in an image relative to the noise that distorts it [13]. It is expressed in decibels (dB) and is calculated as:

$$\text{PSNR} = 10 \log_{10} \left(\frac{R^2}{\text{MSE}} \right) \tag{6}$$

where:

- R is the maximum possible pixel value of the image (here, 255 for an 8-bit image).

Higher PSNR values indicate better image quality, as they signify less distortion in the denoised image compared to the original.

Structural Similarity Index (SSIM) evaluates perceived changes in structural information, luminance, and contrast between two images [14]. It is defined as:

$$\text{SSIM}(x,y) = \frac{(2\mu_x\mu_y + a)(2\sigma_{xy} + b)}{(\mu_x^2 + \mu_y^2 + a)(\sigma_x^2 + \sigma_y^2 + b)} \tag{7}$$

where:

- μ_x and μ_y are the average pixel values of images x and y,
- σ_x^2 and σ_y^2 are their variances,
- σ_{xy} is the covariance between x and y,
- a and b are small constants to stabilize division.

SSIM values range from -1 to 1, where a value of 1 indicates perfect structural similarity. Unlike MSE and PSNR, SSIM provides a more perceptually relevant assessment of image quality, as it incorporates human visual perception in its calculations.

III. Dataset and Result Analysis

A. Experimental Data

The brain tumor MRI dataset from figshare [9] was chosen for this study, consisting of 3,064 MRI images. Six separate tests were carried out on a single image from this dataset.

B. Experimental Configuration & Evaluation

Table I demonstrates the addition of Gaussian noise and provides metrics that highlight the differences between the original sample and the noisy image sample in each experiment. The denoising experiment aims to reduce the mean squared error while increasing both the structural similarity index and the peak signal-to-noise ratio. Additionally, Table I shows the optimal combinations identified in each experiment for effective denoising the noisy images.

Gaussian noise with $\mu = 0$ and varying σ was added to a sample image, which was decomposed up to level 5 using the db3, bior6.8, and sym4 wavelets. The optimal thresholds were determined using the Bayes and Universal methods, and both hard and soft thresholding were applied. The findings for each experiment are summarized below:

1) **Experiment 1** ($\sigma = 10$, Bayes method): The best result was achieved at level 2 with the sym4 wavelet, producing identical outcomes for hard and soft thresholding. Results are shown in Figure 2.
2) **Experiment 2** ($\sigma = 10$, Universal method): The optimal configuration was at level 4 with the db3 wavelet and soft thresholding. Results are shown in Figure 3.
3) **Experiment 3** ($\sigma = 15$, Bayes method): Level 2 with the sym4 wavelet yielded the best results, with identical outcomes for hard and soft thresholding. Results are shown in Figure 4.
4) **Experiment 4** ($\sigma = 15$, Universal method): The best performance was at level 3 using the db3 wavelet and hard thresholding. Results are shown in Figure 5.
5) **Experiment 5** ($\sigma = 25$, Bayes method): Level 2 with the sym4 wavelet produced the best results, with identical outcomes for both thresholding methods. Results are shown in Figure 6.
6) **Experiment 6** ($\sigma = 25$, Universal method): The optimal configuration was at level 4 with the db3 wavelet and soft thresholding. Results are shown in Figure 7.

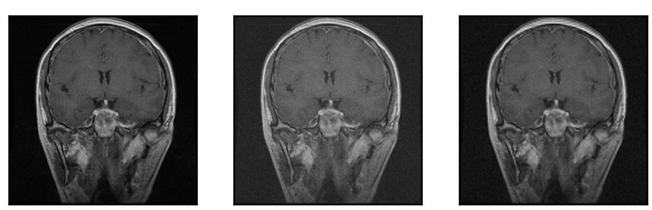

(a) (b) (c)

Fig. 2. Experiment 1 – (a) Original Image, (b) Noisy Image($\mu = 0$, $\sigma = 10$), (c) Denoised Image (with threshold value τ_{bayes})

TABLE I
NOISE SETTINGS AND THE OPTIMAL DENOISING CONFIGURATION FOUND IN EXPERIMENTS

Exp. no	Noise Setup				Optimal Denoising Configuration with Observed Metrics						
	Noise standard deviation (σ)	Noise Metrics			Decomposition level	Wavelet	Thresholding value	Thresholding method	Denoising Metrics		
		MSE	SSIM	PSNR					MSE	SSIM	PSNR
1	10	761.108	0.5	19.316	2	sym4	τ_{bayes}	hard, soft	105.297	0.782	27.907
2	10	725.131	0.493	19.527	4	db3	$\tau_{universal}$	soft	78.128	0.784	29.203
3	15	1148.059	0.385	17.531	2	sym4	τ_{bayes}	hard, soft	198.016	0.711	25.164
4	15	1492.804	0.373	16.391	3	db3	$\tau_{universal}$	hard	108.145	0.74	27.791
5	25	2513.741	0.252	14.128	2	sym4	τ_{bayes}	hard, soft	487.683	0.597	21.249
6	25	2901.145	0.259	13.505	4	db3	$\tau_{universal}$	soft	196.635	0.656	25.194

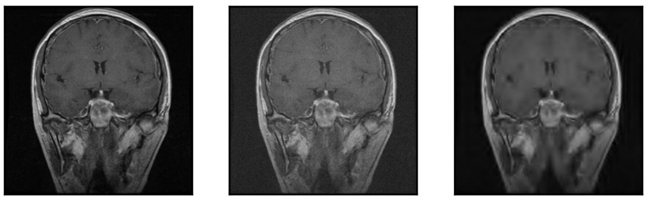
(a) (b) (c)

Fig. 3. Experiment 2 – (a) Original Image, (b) Noisy Image($\mu = 0$, $\sigma = 10$), (c) Denoised Image (with threshold value $\tau_{universal}$)

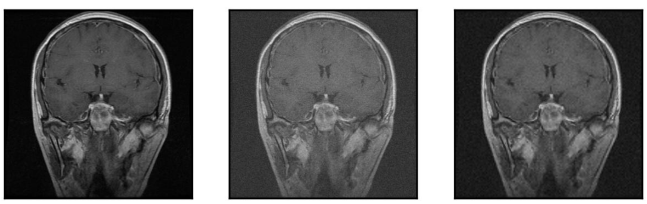
(a) (b) (c)

Fig. 4. Experiment 3 – (a) Original Image, (b) Noisy Image($\mu = 0$, $\sigma = 15$), (c) Denoised Image (with threshold value τ_{bayes})

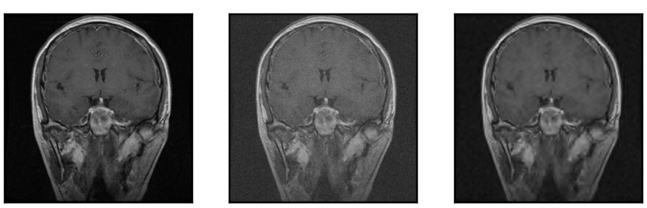
(a) (b) (c)

Fig. 5. Experiment 4 – (a) Original Image, (b) Noisy Image($\mu = 0$, $\sigma = 15$), (c) Denoised Image (with threshold value $\tau_{universal}$)

C. Result Discussion

Figures 8, 9, and 10 illustrate the results of noise mitigation when comparing the original images to the noisy and denoised versions. The configurations observed in denoising, as indicated in Table I, suggest that when the optimal threshold value is determined using the Bayes method, the sym4 wavelet provides the best performance. Conversely, the Universal method

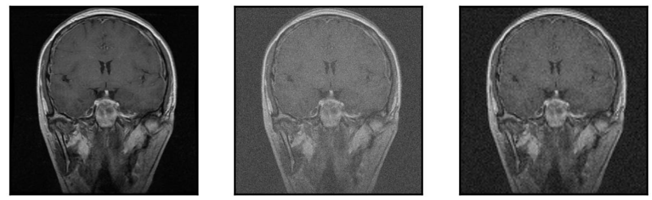
(a) (b) (c)

Fig. 6. Experiment 5 – (a) Original Image, (b) Noisy Image($\mu = 0$, $\sigma = 25$), (c) Denoised Image (with threshold value τ_{bayes})

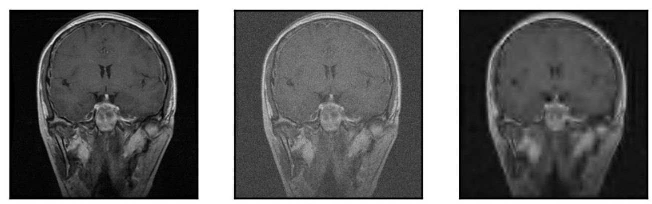
(a) (b) (c)

Fig. 7. Experiment 6 – (a) Original Image, (b) Noisy Image($\mu = 0$, $\sigma = 25$), (c) Denoised Image (with threshold value $\tau_{universal}$)

performs more effectively with the db3 wavelet. Among the various thresholding techniques, the combination of the

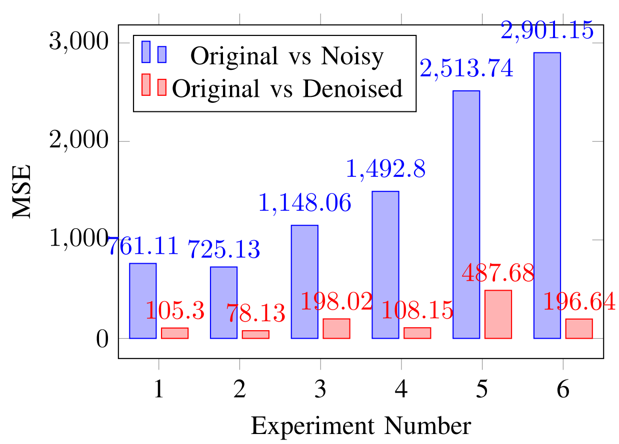

Fig. 8. Comparison of MSE before and after denoising across experiments

Universal threshold and the db3 wavelet achieves the highest PSNR values. Specifically, for noise standard deviations of $\sigma = 10, 15, 25$, the best PSNR values obtained using the db3 wavelet with the Universal method are 29.203 dB, 27.791 dB, and 25.194 dB, respectively.

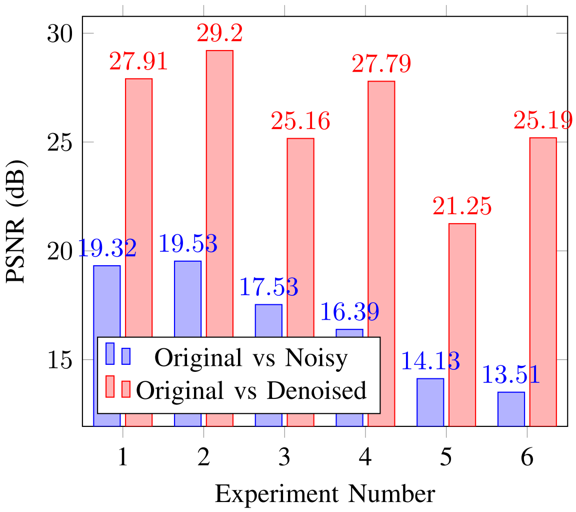

Fig. 9. Comparison of PSNR before and after denoising across experiments

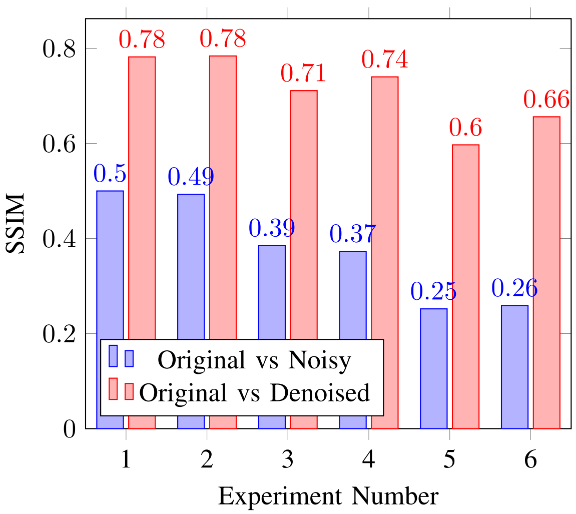

Fig. 10. Comparison of SSIM before and after denoising across experiments

IV. Conclusion

This research developed an effective medical image denoising pipeline using wavelet transformation techniques. Our experimental results on brain MRI images demonstrated that the db3 wavelet with Universal thresholding achieved optimal denoising performance, with PSNR values of 29.203 dB, 27.791 dB, and 25.194 dB for noise standard deviations of σ = 10, 15, and 25 respectively. The sym4 wavelet with Bayes thresholding also showed consistent performance with significant SSIM improvements. Lower decomposition levels (2-4) provided better denoising results across all noise levels. The Universal method with db3 wavelet achieved the highest PSNR values while maintaining structural similarity even at high noise levels (SSIM: 0.656 at σ=25). These results demonstrate the effectiveness of our approach in preserving diagnostic features while reducing noise artifacts. Future work will focus on integrating these wavelet-based techniques with deep learning methods to develop more robust solutions for medical image denoising.

Acknowledgment

We would like to express our gratitude to the Institute of Research and Training (IRT) and IoThink Lab at Hajee Mohammad Danesh Science and Technology University (HSTU) for their invaluable support during this study.

References

[1] S. Kollem, K. R. Reddy, and D. S. Rao, "A novel diffusivity function-based image denoising for mri medical images," *Multimedia Tools and Applications*, vol. 82, pp. 32057–32089, Sep 2023.

[2] T. Guo, T. Zhang, E. Lim, M. López-Benítez, F. Ma, and L. Yu, "A review of wavelet analysis and its applications: Challenges and opportunities," *IEEE Access*, vol. 10, pp. 58869–58903, 2022.

[3] R. Patil and S. Bhosale, "Efficient denoising of multi-modal medical image using wavelet transform and singular value decomposition," in *2023 IEEE IAS Global Conference on Emerging Technologies (GlobConET)*, pp. 1–6, 2023.

[4] Y. Zhang, T. Liu, F. Yang, and Q. Yang, "A study of adaptive fractional-order total variational medical image denoising," *Fractal and Fractional*, vol. 6, no. 9, 2022.

[5] W. El-Shafai, S. A. El-Nabi, E.-S. M. El-Rabaie, A. M. Ali, N. F. Soliman, A. D. Algarni, and F. E. A. El-Samie, "Efficient deep-learning-based autoencoder denoising approach for medical image diagnosis," *Computers, Materials & Continua*, vol. 70, no. 3, pp. 6107–6125, 2022.

[6] S. Izadi, D. Sutton, G. Hamarneh, and et al., "Image denoising in the deep learning era," 2022. PREPRINT (Version 1) available at Research Square.

[7] C. Tian, M. Zheng, W. Zuo, B. Zhang, Y. Zhang, and D. Zhang, "Multi-stage image denoising with the wavelet transform," *Pattern Recognition*, vol. 134, p. 109050, 2023.

[8] L. Gondara, "Medical image denoising using convolutional denoising autoencoders," in *2016 IEEE 16th International Conference on Data Mining Workshops (ICDMW)*, pp. 241–246, 2016.

[9] J. Cheng, "Brain Tumor Dataset," Apr. 2017. [Online; accessed 1-July-2023].

[10] H. A. Chipman, E. D. Kolaczyk, and R. E. McCulloch, "Adaptive bayesian wavelet shrinkage," *Journal of the American Statistical Association*, vol. 92, pp. 1413–1421, 1997.

[11] D. L. Donoho and I. M. Johnstone, "Ideal spatial adaptation by wavelet shrinkage," *Biometrika*, vol. 81, pp. 425–455, 09 1994.

[12] D. Donoho, "De-noising by soft-thresholding," *IEEE Transactions on Information Theory*, vol. 41, no. 3, pp. 613–627, 1995.

[13] Z. Wang and A. C. Bovik, "Mean squared error: Love it or leave it? a new look at signal fidelity measures," *IEEE Signal Processing Magazine*, vol. 26, no. 1, pp. 98–117, 2009.

[14] Z. Wang, A. Bovik, H. Sheikh, and E. Simoncelli, "Image quality assessment: from error visibility to structural similarity," *IEEE Transactions on Image Processing*, vol. 13, no. 4, pp. 600–612, 2004.

[15] A. Shukla, K. Seethalakshmi, P. Hema, and J. C. Musale, "An effective approach for image denoising using wavelet transform involving deep learning techniques," in *2023 4th International Conference on Smart Electronics and Communication (ICOSEC)*, pp. 1381–1386, 2023.

[16] C. Tian, M. Zheng, W. Zuo, B. Zhang, Y. Zhang, and D. Zhang, "Multi-stage image denoising with the wavelet transform," *arXiv*, Sept. 2022.

[17] W. Jifara, F. Jiang, S. Rho, M. Cheng, and S. Liu, "Medical image denoising using convolutional neural network: a residual learning approach," *The Journal of Supercomputing*, vol. 75, pp. 704–718, Feb 2019.